OBSERVATION OF THE HARD DISRUPTION INSTABILITY IN THE IR-T1(IRAN-TOKAMAK 1)

M. Ghoranneviss[1], M. Masnavi[1]*, A. Anvari[2] and D. Dorranian[1]

[1]*Plasma Physics Research Center of I.A.U. (Islamic Azad University), Poonak, Hessarak, P.O.Box 14835-159, Tehran, Islamic Republic of Iran*
[2]*Physics Department, Sharif University of Technology, Tehran, Islamic Republic of Iran*

Abstract

In this article, some diagnostic systems and the preliminary results of the IR-T1** (Iran-Tokamak 1) are presented. Different diagnostic methods, including an array of soft X-ray detectors, visible spectrometer, electron cyclotron emission detector and electromagnetic measurement systems have been used and the hard disruptive instability occurring in the IR-T1 plasma during an ohmic heating discharge, under a range of reproducible conditions for $3 \geq q(a) \geq 2$, is studied. It is found that the disruption activity occurs when the value of the safety factor at the plasma edge becames less than $q(a) \leq 2.7$.

Introduction

The IR-T1 is a small air-core transformer tokamak with circular cross section and without conducting shell and divertor. Its aspect ratio is R/a= 45 cm/12.5 cm. The operation regime according to the original design is q(a)>3.0 (where q(a) is the safety factor at the plasma edge) [1-3].

The major goal of this paper is to study the hard disruptive instability occurring in the IR-T1 plasma, which limits the maximum plasma current and the plasma density [4-6]. It has been known that the global magnetohydrodynamic (MHD) equilibrium of a tokamak is subjected to various forms of instability whose growth rates depend on the local values of the plasma gradient, magnetic shear, current density, etc. [7]. These give rise to perturbations which have the general form:

$$\xi = \xi_0 \exp\{i(m\theta - n\phi + \omega t)\} \qquad (1)$$

with helical structures which generally are most pronounced on or close to these surfaces at some radius (r), where the field line helicity matches that of the mode. If m and n are small integers, these are known as 'rational surfaces' and satisfy the condition $q(r)=m/n$, while m and n are respectively referred to as the poloidal and toroidal mode numbers. Here, θ and ϕ are poloidal and toroidal angles, respectively. These small non-axisymmetric fields are resonant at low-order rational surfaces (safety factor q= 1,2,3...) in the plasma [8]. In the $q(a) \geq 2.0$ disruption, there is a q=2 rational surface which is the pre-condition of the growth of m/n=2/1 Mirnov oscillation [1,9-10] related to most of these kinds of disruptions. This mode couples with the q=2 surface which is the location of a strong plasma Mirnov instability. Mirnov oscillations in

Keywords: Hard disruptive instability; Mirnov Oscillation; Tearing modes; Tokamak

*To whom all correspondence should be addressed

**The IR-T1 is HT-6B Tokamak. This tokamak was delivered to the Azad University of Iran from the Academia Sinica, Institute of Plasma Physics, (ASIPP) of China in 1995.

tokamak plasma are commonly explained by the tearing mode theory [1,11]. Each mode (in particular the current and flow fluctuations related to it), characterized by the poloidal and toroidal mode numbers m and n, is localized around its corresponding resonant surface. It is only when the amplitudes of the tearing modes becomes large enough that the resulting magnetics islands begin to overlap, that the coupling between different modes becomes strong and leads to a disruption [9-16]. The chain of events altogether called 'disruption' is discussed in [16-20], the main phases of which are; I initiating event; II thermal quench and III current quench.

Since mainly in the regime of $q(a) \leq 4$, the most important modes of concern here are $m/n=3/1$, the resonant is on the $q=3$ surface, 2/1 on $q=2$, and 1/1 is associated with $q \leq 1$.

The next section illustrates the main diagnostic systems in our experiment. Another section describes the typical experimental observations in disruption event and results. These results were obtained during one year of operation (1996) without using resonant helical fields (RHFs) and have been restricted to those shots which produced consistent and reproducible data.

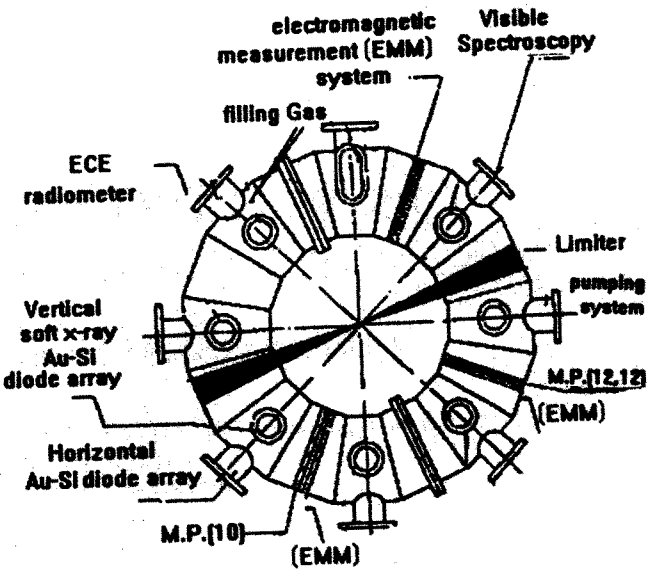

Figure 1. Plan of the IR-T1 showing the configuration and diagnostic positions such as, the Mirnov coils, ECE radiometer system, visible spectrometer and the two soft X-ray detector arrays used for detecting the MHD activity, relative to the limiter.

Diagnostics

Different diagnostic methods which we have used include: soft X-ray (SXR), electron cyclotron emission (ECE) and visible radiations emitted by the plasma and magnetic field measurements. Figure 1 shows the top view of the IR-T1 tokamak and the diagnostic systems on it.

Soft X-Ray Detectors

The principal detector array on the IR-T1 employs 23 silicon surface barrier detectors (ORTEC type TB-18-25-300) which view the plasma through a common window. This consists of a horizontal slit, 3 × 25 mm, covered with a 3 μm thick formver absorption foil with aluminum coating (4000 Å thick) to exclude the visible light and vuv line radiation [21,22]. The sensitive area of each detector element is about 50 mm². Each detector thus views a different chord through the plasma column whose minimum radii are respectively -11,-10,...,+10,+11 cm above the median plane of the plasma. The X-ray flux received by each diode is then due to the X-ray emission integrated along the chord for the whole volume viewed by the detector. A second array of similar design, but with 13 detectors viewing only the lower half of the plasma, is located 90° poloidally from the above array. The response of both X-ray systems is limited at low energies by the absorption of the formver window and at high energies by the thickness of the silicon detector. The energy range of the detected soft X-ray is about 600 eV to 20 keV. The signals are digitized with 8 bit accuracy by means of a data acquisition system.

Visible Spectrometer

To study the behavior and monitor the visible line emissions, Hα, Hβ, and some of the line intensities of light impurities, e.g. carbon, oxygen and nitrogen atoms, a visible (or near ultraviolet) spectrometer with a wavelength range of between 3000Å-7000Å and 0.6 cm space resolution, in which there is a two-lens image system in front of the spectrometer entrance slit and a multichannel optical fiber attached to its exit slit is used.

Electron Cyclotron Emission (ECE) Detector

Second harmonic X-mode ECE from plasma is measured by a 5-channel heterodyne radiometer with corresponding frequency in Ka-band range. Each channel contains a gundiod, local oscillator with a fixed frequency of 35-39 GHZ, attenuator, mixer and directional coupler. ECE signal is received by pyramid horn followed by X-band wave guides, then converted into an intermediate frequency by mixer.

Magnetic Measurement System

Figure 1 shows the positions of the various arrays of coils, which are all oriented to respond to the time varying poloidal field components (B_θ), as mounted

around the torus. These components are conveniently studied with small magnetic search coils, sometimes referred to as 'Mirnov coils' [7]. These arrays are toroidally and poloidally distributed; one (known as the M(12,12)) contains 12 radial and 12 poloidal coils. Another array, M(8), consists of eight poloidal coils around the outside of the vessel. The frequency response of the coils and their output circuit are flat (i.e. signal proportional to frequency) up to at least 30 kHz, the highest frequency of interest in IR-T1 experiments. The signals from each coil are digitally recorded, normally at 250 kHz sampling rate. Also, other magnetic measurement systems which include: 10 Rogowsky coils, 8 loop lines and 2 sine saddle coils 2 cosine coils, are used to measure the plasma current, loop voltage and horizontal displacement of the plasma, respectively.

Description and Discussion of the Experimental Results

The major parameters of the IR-T1 are: Ip≤49 kA, Bϕ= 5-9 kG, $\bar{n}_e$ = (0.7-3) × 10^{13} cm^{-3}, Te(0)= 130 - 250 eV, Ti(0)= 50-80 eV, Zeff ≤ 2 [1], discharge duration is about 20 ms and its plateau phase is about T= 6 ms. Other parameters of the IR-T1 are summarized in Table 1. These parameters are compared with three different and well-known tokamaks.

The observations described here have all been made within the following experimental parameters before disruption activity:

Major radius	R= 45 cm
Plasma current	Ip ≈ 45 kA
Toroidal field	Bϕ ≈ 0.55 tesla
Pulse duration	T ≈ 15 ms
Central electron temperature	Te(0) ≈ 175 eV
Line average central electron density	$\bar{n}_e \approx 1.1 \times 10^{13}\ cm^{-3}$
Impurity level	Zeff ≤ 1.7

Figure 2 shows the typical hard disruption waveform occurring in a discharge with q(a)≅2.2-2.5 in the plateau phase of the IR-T1 (in this paper, we have followed convention by defining q(a) in its cylindrical approximation; $q(a) = 2\ \pi B\phi\ a^2/\mu_0\ Ip\ R$.). Several characteristic features of the hard disruption instability are identified as follows; Figure (2-a): The major decrease in the plasma current after two small positive spikes, the so-called vertex, are close to 12.2 and 12.5 ms. (2-b): A series of negative spikes on the loop voltage (especially two strong negative spikes corresponding to plasma current vertices) are shown. (2-c): The measured horizontal displacement shows that the plasma has an

Table 1. Comparison between the basic characteristics of the IR-T1 with some of typical tokamaks

Machine	R (cm)	B_ϕ (kG)	Ip (kA)	Vloop (v)	Te(0) (keV)	ne(×10^{13}) (cm^{-3})	τe (ms)	SXR sawtooth freq. (kHz)	small oscillation freq. (kHz) on SXR	m=2 mode freq. (kHz)	Gas	Ref.
PLT	130	35	500	2	0.85	14	9	0.11	2-3	2-3	He	8
TFR	98	25	200	2.5	1.2	4.5	2.5	0.4-1	5-10	10-16	H2	9
TOSCA	30	4	8	2	0.2	1.5	0.12	5-10	40-60	40-60	H2	10
IR-T1	45	5-9	20-50	1.2-2	0.2	0.7-3	0.5-2.5	2-5	20-25	20-25	H2	1, 21,22

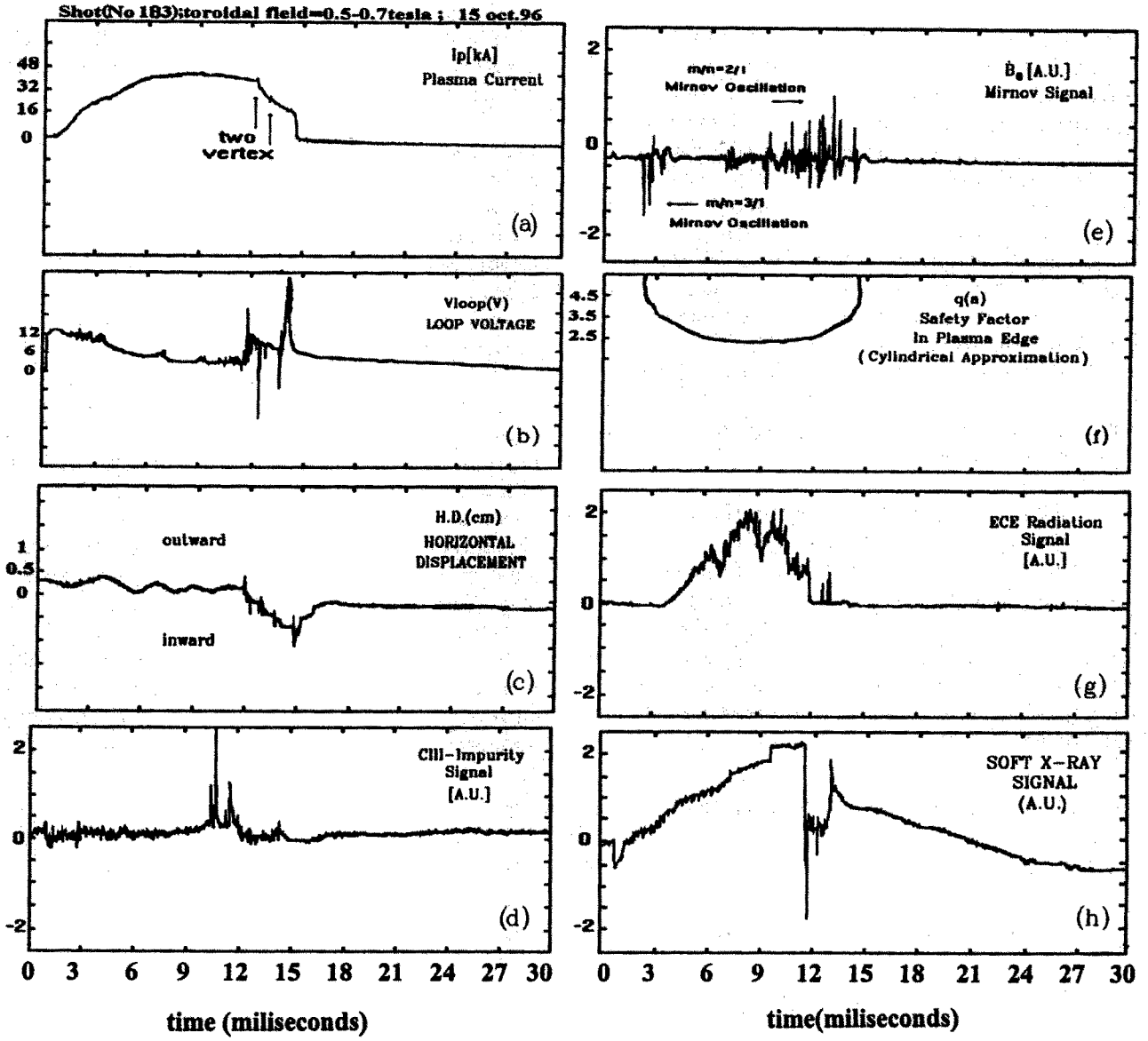

Figure 2. The typical time evolutions of plasma parameters in disruption event on the IR-T1 tokamak: (a) plasma current (kA); (b) loop voltage (v); (c) horizontal displacement signal (cm); (d) CIII-impurity signal (arb. u.); (e) Mirnov coil signal (arb. u.); (f) the safety factor at the plasma edge (in cylindrical approximation); (g) ECE radiation (arb. u.); and (h) central soft X-ray signal (arb. u.). The hard disruptive instability appears close to 12 ms. Disruption occurs during ramp-down of plasma current, that is caused by the decrease in the safety factor at the plasma edge. Positive plasma current spike and negative loop voltage spikes are clearly observed.

inward motion due to instability. As shown, when the plasma is pushed inwards in major radius it causes a positive spike on the loop voltage. (2-d): An enhanced interaction between the plasma and the limiter which is evident by an increase in the release of impurity shown by an increase in the emission of the CIII (λ= 4644 Å, 2s3s-2s3p)-impurity line, starting a few milliseconds before the appearance of the negative voltage spike, and initial plasma current vertex. (2-e): Typical dominant Mirnov oscillations (m/n=3/1 and m/n=2/1) on Mirnov signal, which were measured by one of the external poloidal field coils, are shown. In the ramp-up phase, the dominant mode is m/n= 3/1, while the m/n=2/1 mode has a relatively low amplitude up to three milliseconds before the disruption. In this moment it started to grow in amplitude. As can be seen from this figure, the disruption begins from a phase (I) of the MHD instability development. Usually, this is the m/n= 2/1 mode [23]

with relatively low amplitude as can be seen from the signal of Mirnov coil (≈ 7-9 ms). In this time, the safety factor in plasma edge is about 2.3, as shown in Figure (2-f). The decrease of the electron temperature is shown by a sudden drop in the electron cyclotron emission (ECE) of the plasma, as shown in Figure (2-g). Before disruption, the ECE radiation from the plasma centre shows sawtooth-like oscillations which affect the central part of the discharge and level the electron temperature. The ECE intensity decays with the development of the m/n=2/1 instability and precursors of disruptive energy loss in the central part of the plasma appear. Deep dips in the ECE emission (close to points of 6.5, 9.5, 11 and 12.1 ms) indicate a strong loss of plasma energy.

Figure 3 shows the electron temperature development (arbitrary units) as a function of minor radius at three different times before disruption event. This figure, which is obtained by means of a 5-channel heterodyne ECE diagnostic system, is quite in accordance with the above results. Figure (2-h) shows that the soft X-ray signal exhibited sawtooth-like oscillations from approximately 3 to 9 ms. The major disruption is also recognized by the sudden drop in the central soft X-ray emission close to 12 ms. After the main burst, the temperature in the plasma interior dropped significantly. In addition, at phase II of the disruption, a relatively fast plasma energy release occurs as can be seen on ECE and SXR signals close to 12 ms. After a phase of heat release, current quench occurs which is in turn after vertex and negative loop voltage spike. A few microseconds after initial plasma current vertex, the sharp spike on SXR and ECE emissions is observed. We think that this event is in the direction of the generation of supra-thermal electrons, as proposed by Shuller [18].

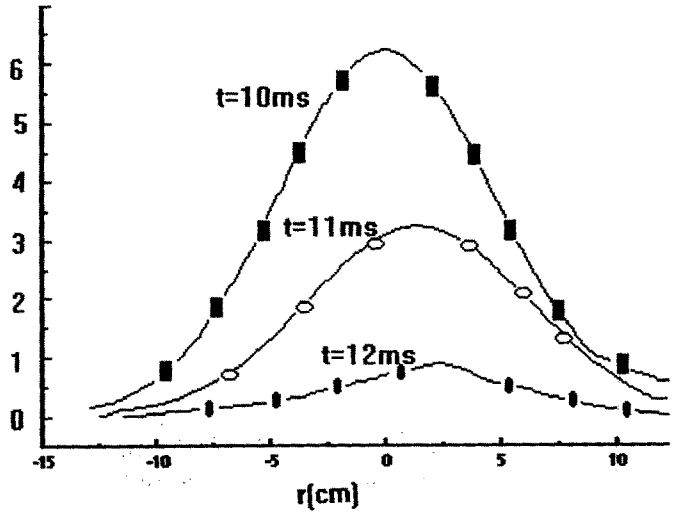

Figure 3. Electron temperature (arbitrary units) as function of minor radius of tokamak at 10, 11 and 12 ms obtained by ECE system.

According to earlier predictions by Callen *et al* [10] and Shuller [18], the timescale of the nonlinear interaction of magnetic islands during thermal quench stage is:

$$\tau_s = (\tau_\eta^3 \ \tau_{A\theta}^{\ 2})^{1/5} \qquad (2)$$

in which τ_η is the magnetic diffusion time and $\tau_{A\theta}$ is the Alfvén time with respect to the poloidal magnetic field. In this case, linear theory predicts a growth rate of $\gamma = \alpha \ \tau_{A\theta}^{\ -2/5} \ \tau_\eta^{\ -3/5}$. Although the growth rate coefficient α depends on the current profile, which is not known, α is of the order of unity [24]. For these parameters, $\tau_\eta = 0.062$s and $\tau_{A\theta} = 1.13 \times 10^{-7}$s, giving a magnetic Reynolds number $S = \tau_\eta/\tau_{A\theta} = 0.55 \times 10^{+6}$.

The range of grossly stable operating conditions can be conveniently described by the so-called "Hugill diagram", as shown in Figure 4. This is a normalized plot of plasma current $[q^{-1}(a) \equiv (\mu_0 R/2\pi a^2 B_\phi) I_p]$ against number density $(\bar{n}_e R/B_\phi)$. It characterizes the radiative properties of plasma respective to the ohmic heating, and it is indirectly bound with the current density profile. To the left of the line OA the density is too low to prevent the current from being carried mainly or wholly by runaway electrons, while to the right of the line OB the density is so high that stable operation is prevented by the disruption of the current channel (for a variety of reasons). The curves OA and OB depend at least to some extent on the degree of plasma purity, and thus on the state of vacuum cleanliness, etc. Therefore, in the IR-T1 tokamak, the disruption instability generally restricts operation to a region $q(a) \leq 2.7$.

Conclusion

We have studied the hard disruptive instability occurring in the IR-T1 plasma during an ohmic heating discharge. It is found that the disruption activity occurs when the value of the safety factor at the plasma edge becomes less than 2.7. In this regime, there is the sequence of the sawtooth-like activity and a strong m/n=2/1 mode, which is similar to many tokamaks and which grows to a large amplitude just before disruption.

Acknowledgements

The authors wish to thank the entire HT-6B Group for installation of the IR-T1, particularly Professor Jikang Xie and Dr. Huang Rong in Academia Sinica, Institute of Plasma Physics (ASIPP), for helpful discussions concerning this tokamak. Thanks and appreciation are also expressed to the National Institute for Fusion Science (NIFS) and the Japan Society for the Promotion Sciences (JSPS) for supporting fully Mr. Majid Masnavi's trip to

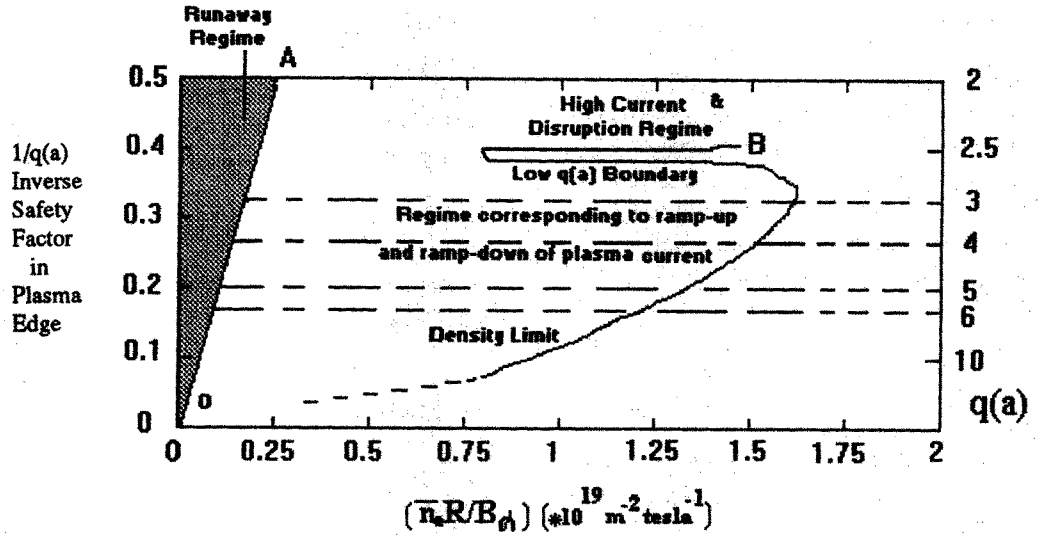

Figure 4. Operation regime (Hugill diagram) for ohmic IR-T1 tokamak. It characterizes the radiative properties of plasma respective to the ohmic heating, and it is indirectly bound with the current density profile. Hugill plot is used to show the accessible operation region of a tokamak for density and current.

China to participate in the '96 Asian Science Seminar on Plasma Physics and Controlled Nuclear Fusion'. Also, the authors would like to thank the technical staff of the laboratory for their upkeep of the IR-T1 tokamak and its systems.

References

1. Chen, J., Xie, J., Huo, Y., Li, L., Zhao, Q. and Zhang, G. *et al. Nuclear Fusion*, **30**, (11), 2271-2284, (1990).
2. Huang, R., Xie, J., Li, Z., He, Y., Wang, S. and Deng, C. *et al. ACTA Physica Sinica*, **2**, (1), 22-30, (1993).
3. Huo, Y.P. *Proceedings of symposium on small scale laboratory plasma experiments*, pp. 52-80. Small Plasma Physics Experiments II, May 15-June 9, ICTP, Trieste, (1989).
4. Callen, J.D. *Lectures on physics models used to describe plasma confinement and heating, JET joint undertaking*, pp. 3.13-3.18. Abingdon, Oxon, U.K., 20th February-20th March, (1987).
5. Kurita, G., Tuda, T., Azumi, M. and Takeda, T. *Nuclear Fusion*, **32**, (11), 18-1911, (1992).
6. Tsuji, S. *Ibid.*, **25**, 305-311, (1985).
7. Cheethman, A.D., Hamberger, S.M., How, J.A., Kuwahar, H., Morton, A.H. and Sharp, L.E. *Australian J. Physics*, **37**, 137-156, (1986).
8. Leuer, J.A., Luxon, J.A. and Antaya, T.A. *Symposium on fusion engineering*, Vol. 2, pp. 1327-1330. September 30-October 5, (1995).
9. Mirnov, S.V. and Semenov, I.B. *Atomnaya Energiya*, **30**, 20, (1971) [*Soviet Atomic Energy*, **30**, 22, (1971)].
10. Callen, J.D., Waddell, B.V., Carreras, B., Azumi, M., Catto, P.J. and Hicks, H.R. *et al. 1978 Proceedings of 7th international conference on plasma physics and controlled nuclear fusion research* (Innsbruck), pp. 415-443, (1978).
11. McGuire, K.M. and Robinson, D.C. *Phys. Rev. Lett.*, **44**, 1666, (1980).
12. Kleva, R.G. and Drake, J.F. *Phys. Fluids B.*, **3**, 372, (1991).
13. Waidmann, G. and Kuang, G. *Nuclear Fusion*, **32**, 645, (1992).
14. Wesson, J. *Tokamaks*, pp. 178-181. Clarendon Press, Oxford, (1987).
15. Manheimer, W.M. and Lashmore-Davies, C.N. *MHD and microinstabilities in confined plasma*, pp. 11-15. IOP Publishing Ltd., UK, (1989).
16. Harley, R., Buchenauer, D.A., Coonrod, J.W. and McCuire, K.M. *Nuclear Fusion*, **29**, (5), 771-785, (1989).
17. Yu, G.Y. *Proceedings of '96 Asian science seminar frontier of physics in fusion relevant plasmas'*, pp. 91-103, 20-29 Oct., Hefei-Tunxi, P.R. China, (1996).
18. Schuler, F.C. *Plasma Physics and Controlled Fusion*, **37**, A135, (1995).
19. Kadomtsev, B.B. *Ibid.*, **26**, 217, (1984).
20. Sauthoff, N.R., Von Goeler, S. and Stodiek, W. *Nuclear Fusion*, **18**, 1445, (1978).
21. Li, L.Z. and Wang, Z. *Chinese Physics*, **6**, (4), 821-828, (1986).
22. Ghoranneviss, M., Abbaspour, A., Anvari, A. and Masnavi, M. *Scientia Iranica*, **4**, (1 & 2), 71-76, (1997).
23. Zhao, Q. and HT-7 Group. *J. Plasma Fusion Research*, **1**, 276-279, (1998).
24. White, R.B. In *Basic plasma physics* (ed. A.A. Galeev and R.N. Sudan), p. 632. North Holland, New York, (1983).